Climate Feedbacks Induced by Stationary Glacial Meltwater Forcing in a Coupled Model of Intermediate Complexity

Flávio Justino

Department of Physics, University of Toronto

M5S 1A7 Toronto, ON Canada

Phone: 1 416 946 7129, FAX: 1 416 978 8905

(fjustino@atmosp.physics.utoronto.ca)

Abstract

Based on coupled model simulations we investigate the atmospheric and oceanic response to sustained glacial freshwater input in the North Atlantic under a glacial background state. The results demonstrate that a weakening of the conveyor belt triggered by weaker density flux leads to rapid changes in global sea-ice volume and reduced poleward heat transport in the Northern Hemisphere (NH). In the Southern Hemisphere (SH), however, the oceanic heat transport increases substantially. As a result, strong cooling occurs over the North Atlantic whereas the SH extratropical region warms up. The suppression of the thermohaline circulation also drastically change the atmospheric circulation. At 800 hPa a vast area over the North Atlantic/Europe sector is dominated by high pressure anomalies whereas negative pressure anomalies act over North America. This in turn induces warm air advection over the eastern portion of North America as well as enhances the transport of warm and salty water from the tropical region to mid-latitudes. Furthermore, calculation of the high pass transient eddy activity in the lower troposphere showed increased (decreased) poleward temperature flux in the NH (SH) due to higher (lower) baroclinic activity. This atmospheric-oceanic interplay opposes the initial climate tendency imposed by the freshwater forcing.

1. Introduction

The past 10,000 years have been anomalous in the history of our planet. This period, during which civilisation developed, was marked by reduced global climate variability, unlike during any similar time span of the past 100 millennia (Broecker (1995)). High-resolution records from ice and sediments cores and other sources have revealed that in the past rapid climate changes occurred at the time-scale of human lives. Some of the most pronounced regional and large-scale climate changes (involving, for example, a regional change in mean annual temperature of several degrees Celsius or dramatic changes in precipitation patterns) occurred within a few centuries, and often within a few decades, or even just within a few years (Alley (2000)).

During the last decade has increase the number of evidence that those climate shifts are related to freshwater anomalies into the Labrador/Nordic Seas (Schäfer et al. (2001), Bond et al. (1997), Blunier and Brook (2001) and Blunier et al. (1998)). Furthermore, Broecker (1994) showed that these vigorous climatic events may be related with instability of the thermohaline circulation (THC). Climate changes associated with perturbation in the THC have been inferred from paleoclimatic records as well as from model simulations forced by increasing greenhouse gas concentrations. For example, the abrupt cold event that occurred between 8.4 and 8.0 kyr can be attributed to a weakening of the THC which was triggered by an abrupt release of the post-glacial Lake Agassiz to the North Atlantic (von Grafenstein et al. (1998)). Similarly, the general temperature pattern of the Younger Dryas as derived from various proxies data e.g. by carbon isotope ratios, shows a close resemblance with coupled atmosphere-ocean modeling experiments that simulate a collapse of the THC (Manabe and Stouffer (1997), Mikolajewicz et al. (1997)). Moreover, paleo-proxy data analyses have suggested that the meltwater pulse II that occurred around 23,000 BP (calender years before present) was characterized by a dramatic nutrient enrichment of Atlantic deep water, which suggest a shutdown of the THC (Crucifix et al. (2002), Schäfer et al. (2001)). Reduction of the North Atlantic Deep Water (NADW) formation rate has been simulated by freshwater inflow to the North Atlantic, either from glacial melting

(e.g. Knutti et al. (2004), Broecker (1994)), or from ice sheet instabilities (e.g. MacAyeal (1993)). Recently, Timmermann and Goosse (2004) demonstrated that wind-forcing is a crucial element to sustain meridional overturning circulation. In fact, in their study neglecting wind-stress over the North Atlantic led to a complete shutdown of the conveyor belt circulation. Previous attempts to quantify the impact of wind driven circulation on the THC (e.g. Schiller et al. (1997), Oka et al. (2001)) also pointed out that Ekman dynamics in the sub-tropical gyre plays a key role to stabilize the THC.

The present day hydrological cycle is in balance over annual time scales, with evaporation over the ocean replenished by marine precipitation and continental runoff, as discussed by (Marshall and Clarke (1999)). Nevertheless, a different treatment is required for Pleistocene studies due to the modified hydrological cycle and topographic features. Bjerknes (1964) proposed that a weakening of the oceanic heat transport, perhaps triggered by a shutdown of the NADW, leads to a cooling of the northern North Atlantic, which in turn increases the baroclinicity and the transient eddy activity in the atmosphere. This may subsequently lead to a warming of the northern North Atlantic opposing the initial cooling tendency (see Fig. 1). This web of climate interaction proposed in the Figure 1 can be investigated in details by coupled model simulations mimicking a climate state perturbed by a substantial weakening of the THC.

Hence, this study addresses the impact of the stationary freshwater inflow into the North Atlantic on the atmosphere-sea-ice-ocean system based on 5 sensitivity experiments. This work is motived by the fact that the behavior of the air-sea mechanism proposed in Figure 1 has not been studied in details in a glacial environment. It has also been argued that model simulations conducted under anomalous deep water formation rate can improve our understanding of climate feature characteristic of stadial periods (e.g. Heinrich events). Moreover, previous experiments concerning the climate response to perturbation in the THC (e.g. Seidov et al. (2001), Stocker (1998), Mikolajewicz et al. (1997), Manabe and Stouffer (1995)) have been set up from a climate state driven by present day or pre-industrial boundary conditions. Thus, their interpretation of the climate response in paleoceanographical terms is weaken.

The paper is organized as following: Section 2 describes the coupled atmosphere-ocean-sea-ice model and the experimental design. Section 3 investigates the impact of freshwater flux upon the thermohaline circulation, the heat transport and the atmospheric circulation. In addition, this section provides a brief discussion of the predicted interhemispheric seesaw as well as focuses on changes in the baroclinic activity and the transients eddies. Finally, the summary and concluding remarks are presented in Section 4.

2. The Coupled Climate Model and the Design of the Numerical Experiments

The atmospheric component ECBILT (Opsteegh et al. (1998)) of our coupled model is a 3-layer model with a quasi-geostrophic adiabatic core (Marshall and Molteni (1993)) and a set of physical parametrizations for the hydrological cycle (Held and Suarez (1978), Opsteegh et al. (1998)) and a simplified radiation code. It is a spectral model that is run at T21 triangular truncation, which corresponds to an approximate resolution of 5.6^0 in both latitude and longitude. The coupled ocean-sea ice model CLIO (Goosse et al. (1999), Goosse and Fichefet (1999), Goosse et al. (2002)) is based on the primitive equations and employs a free surface for the ocean component and thermodynamic/dynamic assumptions for the sea-ice component. A parameterization for vertical mixing (Goosse et al. (1999)) is employed that constitutes a simplification of the Mellor and Yamada 2.5-level turbulence closure scheme (Mellor and Yamada (1982)). Furthermore, the ocean model CLIO includes mixing along isopycnals so as to capture the impact of meso-scale eddies on the transport (Gent and McWilliams (1990)) as well as the flow of dense water down topographic features (Campin and Goosse (1999)). The horizontal resolution of the CLIO model is 3° and there are 20 unevenly spaced vertical levels in the ocean. The individual models are coupled through exchanges of momentum, freshwater and heat and the simulations are performed using weak freshwater flux corrections so as to inhibit climate drift (Marotzke and Stone

(1995)). The model is highly efficient computationally such that on a DEC-alpha workstation, a 150-year-long simulation may be performed within a single day.

In order to analyze the climate response to freshwater input, five experiments are performed: a simulation of the present day climate, a simulation focusing on the last glacial maximum (LGM), and three additional freshwater experiments driven by LGM boundary conditions. The freshwater experiments are carried out with different sustained freshwater input (FI), i.e. between 50°N and 70°N the amount of FI into the North Atlantic was altered adding 0.19, 0.38 and 0.475 Sv ($1Sv = 10^6 m^3 s^{-1}$). It represents for each model grid cell an increase of FI up to 0.16×10^{-7}, 0.33×10^{-7} and 0.42×10^{-7} Sv, respectively ($0.19FI$, $0.38FI$ and $0.47FI$ hereafter). The amount of freshwater input is based on previous simulation (Rind et al. (2001a), Manabe and Stouffer (2000), Schiller et al. (1997), Manabe and Stouffer (1997)) as well as on observed estimates from either glacial meltwater (Liccard et al. (1999)) or ice rafted debris (MacAyeal (1993)). The FI experiments have been run for 700 years starting from equilibrated LGM climate conditions. It is important to note that the LGM simulation was integrated for 10,000 years. The analyses discussed here are based upon the last 300 years of each simulation. The present day and LGM simulations have been discussed in detail in previous studies (Justino et al. (2005), Timmermann et al. (2004)). The LGM run and the FI experiments employ the reconstructed ice sheet topography (ICE-4G) characteristic of 21,000 BP (Peltier (1994)), reduced atmospheric CO_2 concentration (200 ppm), and appropriate LGM orbital forcing (Berger (1978)). Moreover, an appropriate LGM vegetation mask is prescribed (e.g. Crowley (1995)), for which the deforested soils and plant cover are replaced by their respective glacial albedos. The incorporation of the influence of the ice sheet albedo increases the surface albedo by more than 60% in North America and northwestern Europe. In comparison with the predicted present day climate, the LGM simulation exhibits an overall surface cooling except over the North Pacific that is mainly driven by topographically-induced modification of the large-scale atmospheric circulation (for details see Timmermann et al. (2004)). The simulated rainfall anomalies are consistent with lake level reconstructions of Kohlfeld and Harrison (2000), and a permanent La Niña pattern. The comparison between the

simulated temperature and the paleo-reconstructions shows good agreement in the equatorial zone. Over the subtropics, however, the model underestimates the cooling.

The SSTs anomalies are in good agreement with the CLIMAP (1981) and GLAMAP (Schäfer-Neth and Paul (2003)) reconstructions (not shown). Similar previous LGM simulations (e.g. Cook and Held (1988) and Rind (1987)), we found that the presence of Laurentide ice sheet generates an upstream blocking situation whereas a downstream low takes place over North Atlantic (Fig. 2).

3. Results and Discussion

a. *Thermohaline Circulation*

Compared to reality, the ECBilt-Clio overestimates the strength of today's NADW. The simulated present day transport associated with the NADW (24 Sv) is around 30% larger than that observed (18 Sv) (Talley et al. (2003), Hall and Bryden (1982)). This higher NADW formation rate is a result of the increased thermal contribution to density changes as well as due to overestimated sea-ice volume and subsequently of much higher extra-tropical surface salinity/brine rejection (Justino et al. (2005)). It must be noted, however, that discrepancies associated with the strength of the NADW have been found in models of different complexity, as discussed by Houghton et al. (2001). Shown in Figure 3 is the simulated NADW and the Antarctic Bottom Water (AABW) in the FI experiments and the LGM run. Compared to the simulated present day NADW the LGM simulation predicts stronger NADW mainly due to increased vertical air-sea temperature contrast and thus the loss of heat from the ocean to the atmosphere, which leads to strong convective mixing. Paleoceanographic data (McCave et al. (1995) and Veum et al. (1992)) and other LGM model simulations (Hewitt et al. (2001) and Kitoh et al. (2001)), support the possibility of a stronger NADW, as simulated here.

The $0.19FI$ simulation shows a slight reduction of the NADW by about 15% (Fig. 3a). This

THC response is similar the results found by Rind et al. (2001a) that predicted for a freshwater inflow of 0.12 Sv, a 10% reduction of the NADW. The other FI simulations experience larger anomalies. The NADW in $0.38FI$ weakens by about 17 Sv which represents a 40% reduction compared to the LGM reference run. The changes in the $0.47FI$ are even stronger and the NADW drops up to 25 Sv. This represents a reduction of more than 90% of its strength in the LGM simulation. It is important to note that a similar trend is observed in the first 30 years in the three FI experiments. The weakening of the NADW is also accompanied by a strengthening of the AABW (Fig. 3b). Remarkable, however, is the relative magnitude of the changes in the $0.47FI$ run. As a result of the large amount of freshwater employed in this simulation the AABW intensifies by more than 8 Sv. It is twice stronger than that predicted by the present day run and almost four times the LGM counterpart. The changes in $0.19FI$ and $0.38FI$ runs are weaker, by about 2 and 6 Sv, respectively. The associated response of the AABW to the amount of freshwater anomalies in the North Atlantic indicates a strong coupling between the Northern and Southern Hemispheres. Nevertheless, it is evident from Fig. 3 that AABW experiences much larger amplitude changes compared to those related to the NADW.

Changes in surface salinity in the FI experiments are crucial for the weakening of the NADW as well as for the enhancement of the AABW. As proposed by Schmitt et al. (1989) and Speer and Tziperman (1992), surface density anomalies (a combination of the thermal and the haline density anomalies) can generate thermohaline circulation changes. Compared to the LGM simulation, the FI experiments show a reduction of the thermal density flux due to stronger advection of warm air from the east coast of North America and equatorial region. This in turn reduces the air-sea temperature contrast and thus the loss of heat from the ocean to the atmosphere, which leads to shallow convective mixing and subsequently weaker NADW formation rate. In addition, the freshwater input reduces the haline density flux which prevents the water to become dense to sink. This happens in the main region of deep water formation (not shown).

Rind et al. (2001b) attributed the strengthening of the AABW to changes in the Antarctic Circumpolar Current (ACC) and to the longitudinal heat flux divergence out of the South Atlantic.

Thus, increasing the cooling and sea-ice growth/salinity amplifying the bottom water production. In part this finding can be applied here because the $0.38FI$ and $0.47FI$ experiments exhibit higher sea surface salinity (SSS) (not shown), however, this is not accompanied by an increase in sea-ice and stronger ACC (see Fig. 9a). Calculations of the density flux in the SH show that both, the thermal and haline density flux anomalies lead to the AABW intensification. The FI experiments show large negative heat flux anomalies (i.e. oceanic heat loss) that further increase the thermal density flux. In addition, the reduced precipitation - evaporation flux (by about 10m/100years) strengthens the haline density flux in particular in the Antarctic peninsula.

b. *Atmospheric Circulation*

As proposed by Bjerknes (1964) changes of the poleward heat transport, perhaps associated to distinct NADW formation rate as discussed above, lead to anomalous meridional thermal gradient between equatorial and extratropical latitudes. Indeed, this is depicted by surface temperature anomalies between the FI experiments and the LGM simulation (Fig. 4a,b). It is evident that $0.38FI$ and $0.47FI$ experiments show pronounced cooling in the North Atlantic whereas warmer conditions are predicted in the SH oceans and northeastern Pacific. This bipolar “seesaw” in the Atlantic Ocean has been found in previous studies (e.g. Rind et al. (2001b), Stocker (1998)). It has been shown that on large spatial scale, a shutdown of the THC results in a cooling of the water masses in the North Atlantic, and a warming in the South Atlantic as simulated here. The strong cooling in the FI experiments over the North Atlantic and adjacent areas is in part a result of increased sea-ice volume that insulates the atmosphere from the underlying warmer ocean. Furthermore, the reduced specific humidity (amount of water vapor in the air) also plays a key role in cooling the air due to weaker greenhouse capacity of the dryer atmosphere. It should be noted that the impact of heat transport upon surface climate condition is discussed later. Over the tropical North Atlantic (0-30°N), the lower surface temperature in the FI experiments with respect to the LGM run is associated to enhanced upwelling as a consequence of stronger

northeast trade winds as well as a result of cold air advection from the subtropical region (see Fig. 6a,b). In the SH, on the other hand, the tropical region experiences a slight warming mainly driven by weaker southeast trade winds and consequently reduced upwelling. It is important to note that the surface temperature anomalies over the ocean reproduces mainly changes in sea surface temperature. In general, one can argue that the changes in the NH resemble glacial conditions whereas the changes in the SH could be interpreted as characteristic of inter-glacial periods.

In the *0.47FI* experiment, for instance, the land surface temperature drops up to 6°C over Greenland and Europe, and up to 2°C over Asia from already a very cold LGM climate state (Fig. 4b). This is associated to increased cold advection from the North Atlantic and Arctic Ocean (see Fig. 6a,b). In addition, the sea-ice/snow albedo feedback strengthens the amount of solar radiation reflected to space producing substantial changes in the surface radiative budget. Over southern North America, however, due to the warmer air blowing from the equatorial region the FI experiments show positive temperature anomalies compared to the LGM run. Similar results are also predicted by the *0.19FI* experiment anomalies, however, they show smaller amplitudes. Therefore, they are not shown here.

Over the northeast Pacific the FI experiments exhibit higher surface temperature than those simulated in the LGM run. A similar mechanism responsible for positive surface temperature anomalies between the LGM and the present day climate has been discussed by Timmermann et al. (2004). They argued that SST changes in the North Pacific in the LGM run are primarily driven by modifications of the large-scale atmospheric circulation. Which in turn leads to a reduction of latent and sensible ocean cooling in the subtropical North Pacific. Moreover, reduced wind stress curl over the Kuroshio area slows down the subtropical and subpolar gyre, cooling down the western North Pacific whereas the northeastern Pacific warms up. These features are also found by comparing the FI experiments to the LGM simulation.

Changes of eddy geopotential height (i.e. the geopotential height with the zonal mean removed) are characterized by high pressure anomalies from the North Atlantic to Eurasia,

whereas low pressure anomalies take place over North America and North Pacific (Fig. 5a,b). Therefore, over the western North Atlantic a south-westerlies wind anomalies appear from the sub-tropics to the Nordic Seas (Fig. 6a,b). Hence, according to the Sverdrup relation an enhancement of the wind-driven circulation may be expected. In the upper troposphere, however, a though takes place over the North Atlantic and a ridge is simulated over the North Pacific (not shown), pointing out an intensification in the baroclinic structure of the atmosphere as proposed by Bjerknes (1964) (Fig. 1). This anomaly geopotential feature in the FI experiments reinforces the jet stream over the North Atlantic but weakens it over the North Pacific. In the SH due to reduced meridional thermal gradient the FI experiments show weaker westerlies at 800hPa than those predicted by the LGM simulation. At 200 hPa, however, the jet stream is slight stronger over the Indian/Pacific sector.

c. *Heat Transport*

Although changes in sea surface conditions and atmospheric circulation are crucial to understand the climate, it is important to investigate the impact of freshwater forcing upon the oceanic and atmospheric heat transport. The total poleward heat transport of the atmosphere-ocean system in each latitudinal band is computed from the difference between the net shortwave radiation and the outgoing longwave radiative flux at the top of the atmosphere. It can be expressed as,

$$H(\phi)_{total} = H_{ATM} + H_{OCE} = 2a^2\pi \int_{-\pi/2}^{\phi} (S_{TOA}(\phi)' - L_{TOA}(\phi)') \, .cos\phi' . d\phi' \qquad (1)$$

where, H_{total}, H_{ATM} and H_{OCE} are the total, atmospheric, and oceanic heat transport, respectively. a is the radius of the Earth, ϕ is the latitude, S_{TOA} is the zonally integrated net shortwave radiation, and L_{TOA} is the zonally integrated outgoing longwave radiative flux. Both fluxes are computed at the top of the atmosphere.

The simulated present day total heat transport is comparable to calculations which are based on observed data (Trenberth and Caron (2001), Peixoto and Oort (1992)). The maximum pole-

ward heat transport appears in both hemisphere around 45°N and 45°S and attains maximum values of 5.2 PW $(PW = 10^{15}W)$ (Justino (2004)).

Compared to the LGM simulation, the $0.47FI$ and $0.38FI$ runs show a reduction in the heat transport maxima in the NH by about 1 PW and 0.5 PW, respectively (Fig. 7). Nevertheless, in the SH the differences among the simulations do not show significant changes. Increased freshwater into the North Atlantic clearly affects the oceanic heat transport (Fig. 7b). It is evident the substantial reduction (increase) of the northward (southward) heat transport in the FI experiments. For instance, at 30°N the oceanic heat transport is reduced by 0.63 (0.25) PW in $0.47FI$ ($0.38FI$) run, primarily as a result of changes in the North Atlantic (Table 1). It is interesting to note, however, the enhancement of the oceanic heat transport in the North Pacific which on global basis diminishes the cooling tendency induced by the Atlantic Ocean (Fig. 8b). In addition, it may play an important role in the higher surface temperature over northeast Pacific in the FI experiments with respect to the LGM simulation.

The appearance of southward oceanic heat transport in the $0.47FI$ experiment (Fig. 8a) contrasts with recent observations (Talley (2003)) and modeling results (Böning et al. (1996)) that show northward meridional heat transport in the Atlantic Ocean. Thus, higher SH extratropical surface temperature in the FI experiments compared to the LGM run is primarily a result of the large amount of accumulated oceanic heat in the SH. This is consistent with the hypothesis suggesting that the South Atlantic cools by the existence of the NADW (Stocker and Johnsen (2003), Stocker (1998)).

Changes of atmospheric and oceanic circulations have also a large impact upon the oceanic salt transport due to induced wind-driven circulation anomalies. Compared to the LGM, the FI experiments show strong northward salt transport in the North Atlantic. The maximum northward salt transported in the LGM run attains values of 5 psuSv around 45°N, though it increases up to 16 and 18 psuSv in the $0.38FI$ and $0.47FI$ experiments (Fig. 8c). Furthermore, it is clearly seen the reduction of the southward salt transport. It is important to note that this enhanced salt transport opposes the North Atlantic freshening induced by the freshwater forcing.

d. *Interhemispheric Seesaw*

One of the most important findings in the study of millennial-scale climate events is the out-of-phase climate response of the two hemispheres - the interhemispheric seesaw. Broecker (1998) suggests that for rapid climate changes to be initiated there must be a trigger for a sudden "switching off" or a strong decrease in the rate of deep water formation in either the North Atlantic or the Southern Ocean. This must be due to a decrease in the density of surface water. Changes of the density could result from changes in salinity (changes in fresh water) and/or increased temperatures. The predicted interhemispheric or bipolar seesaw in the FI experiments is shown in Figure 9. It exhibits rapid changes of sea-ice volume in the NH (Fig. 9a) which leads to slight cooling over Greenland (Fig. 9b). It is interesting to note the strong link between the changes in surface temperature in Weddell Sea and the heat transport anomalies at 30°S (Fig. 9b,c). By increasing the heat transport in the South Atlantic by 0.8 PW, the surface temperature over Weddell Sea increases by about 10°C in a period of 300 years. This in turn reduces the sea-ice volume in the Southern Hemisphere (Fig. 9a). In a recent study (Knutti et al. (2004)) showed that the amount of freshwater discharge into the North Atlantic in addition to a reduction in the THC, has a direct impact on the temperature of the Southern Ocean. They demonstrated that the related anomalous southward oceanic heat transport arises from a zonal density gradient in the subtropical North Atlantic caused by a fast wave adjustment process.

e. *Baroclinic Instability and Eddy Activity*

In order to investigate changes in baroclinicity induced by anomaly freshwater forcing as proposed in Figure 1, is computed the Eady growth rate (σ_{BI}). This is a simply measure of the baroclinicity of the atmosphere and can be employed to quantify the potential for instability and cyclone growth (Lindzen and Farrell (1980)). The Eady growth rate estimates baroclinic instability through the vertical wind shear and the static stability in the atmosphere. It is defined as $\sigma_{BI} = 0.31\frac{f}{N}|\partial \mathbf{v}/\partial z|$ where f is the Coriolis parameter, N the Brunt-Väisälä frequency, z

the upward vertical coordinate and $\mathbf{v}$ the horizontal wind. The anomalies between the FI experiments and the LGM are shown in Fig. 10a,b. As expected, the cooling over the North Atlantic/northern Europe induced by enhanced freshwater forcing increases the meridional thermal gradient/vertical wind shear which subsequently produces stronger baroclinic activity (higher σ_{BI}) over that region (Fig. 10a). It is interesting to note that very weak changes are found over the North Pacific as a result of smaller temperature anomalies between the FI experiments and the LGM run (Fig. 4a,b). Homogeneous warming in the SH also leads to substantial reduction of the baroclinic activity over the ACC area (Fig. 10b). Although, higher σ_{BI} is predicted over the Antarctic continent between 0-60°E.

Changes in the baroclinic structure of the atmosphere is tightly linked to anomalies in the mean wind, stationary and transient eddies (or commonly known as storm tracks). In the following, an initial analysis of the subtropical and polar jets is provided by calculating the upper level total kinetic energy [$TKE = \frac{1}{2}(\overline{u^2 + v^2})$]. In the NH is evident an intensification and a northward shift of the maximum TKE (Fig. 10c). Over the North Atlantic this reflects the enhancement of the steady components of the jet stream. This strong jet stream plays an important role in reducing the seasonal zonal thermal contrast in mid-latitudes by coupling the large oceanic heat reservoir to much smaller terrestrial one (Schneider (1996)). Over the North Pacific the changes are more complicated. Due to the weaker subtropical jet a belt of reduced TKE is found around 30°N, whereas as a result of the stronger polar jet the TKE enhances over polar latitudes (Fig. 10c). In the SH (Fig. 10d), the TKE strengthens around Antarctica with two maximum placed over Atlantic and Pacific Oceans, but weaker TKE is found over the Atlantic/Indian Ocean sector.

After discussing the mean wind and stationary waves anomalies, changes in the transient waves are analyzed. In the following, transient eddy activity is analyzed in terms of the upper level (200 hPa) eddy kinetic energy [$EKE = \frac{1}{2}(\overline{u'^2 + v'^2})$], and the low level (650 hPa) eddy temperature flux [$(\overline{v'T'})$], with the overbars denoting the time mean and primes the deviation therefrom. The high pass transient eddies are extracted from daily model data and have been temporally filtered using a high-pass filter to include only systems with growth and decay with

timescales smaller than 6 days. Those changes of the TKE discussed above are not directly linked to changes in the high pass transient kinetic energy (EKE), as can be realized by comparing the Figure 10c,d to the Figure 11a,b. For instance, the high pass transient EKE is reduced over North America in the $0.47FI$ run while the TKE is enhanced (Figs. 10c, 11a). Similar "anti-phase" behavior between the TKE and the high pass transient EKE is clearly seen in the SH (Fig. 10d, Fig. 11b). Compared to the LGM simulation, the FI experiments show stronger high pass transient EKE over the most part of the NH (Fig. 11a). Nevertheless, areas of reduced storm track activity are simulated over North America and the North Atlantic. This feature in the North Atlantic does not agree with the predicted positive Eady growth rate anomalies/higher baroclinic activity (Fig. 10a). This may indicate that enhanced baroclinic activity is confined to the lower troposphere. It is interesting to note the spot of enhanced transient eddies activity over the Bering Strait region (Fig. 11a,c) perhaps associated to the intensified polar jet. There are several reasons for why the zonal mean wind determines transient eddy activity. A strong jet is often associated with increased baroclinic and barotropic instability resulting in enhanced transient wave activity. Furthermore, Trenberth (1991) showed that a strong jet also advects transient wave activity further to the east. In the SH, the upper level EKE is extremely weaker in agreement with the reduced baroclinicity (Fig. 11b). Turning to the changes in the eddy temperature flux [($\overline{v'T'}$)] in the lower troposphere (Fig. 11c,d), it is evident enhanced $\overline{v'T'}$ over the Nordic Seas, Alaska and over the Bering Strait region. In the SH, however, the FI experiments show an overall reduction of the poleward temperature flux.

The analyses of the baroclinic activity and the high pass transient eddies anomalies reveal that increased freshwater input into the North Atlantic leads to enhanced northward temperature flux over the North Atlantic and the North Pacific which favors a warming in the NH. Furthermore, northward warm air advection anomalies also contribute to warm the North Atlantic as shown in Figure 4c,d. In the SH, however, the low level mean circulation and the storm tracks do the opposite, the weaker storm track transports less heat to high latitudes which leads to an extra-tropical cooling. Given that, one may conclude that the high pass transient eddies anomalies in the FI

experiments act as a negative feedback, thereby weakening the climate response associated to the freshwater forcing.

4. Summary and Concluding Remarks

Based upon an equilibrated climate driven by LGM boundary condition is found that the NADW production rate is approximately proportional to the amount of freshwater inflow in the North Atlantic (Rind et al. (2001a), (Manabe and Stouffer (1997), Mikolajewicz et al. (1997)). The weakening of the NADW induces lower SST and air temperature in the NH. In the SH, on the other hand, strong warming is accompanied by an increase in the AABW.

By comparing the density flux in the FI experiments and the LGM simulation (not shown) is argued that changes in the NADW and AABW are mainly driven by modified thermal and haline density fluxes. In the NH, the reduction of the thermal component of the density flux is due to the advection of warm air from the east coast of North America and equatorial region, which subsequently affects the convective mixing. Whereas, the haline density flux reduces as a result of imposed freshwater inflow. In the SH, on the other hand, strong AABW formation rate is associated to large negative heat flux anomalies (i.e. oceanic heat loss) in addition to enhanced haline density flux due to reduced precipitation - evaporation flux.

The shutdown of the THC leads to weaker oceanic heat transport in the North Atlantic by about 1 PW (see Fig. 8a , Table 1). Thus, the most part of the oceanic heat is transported to the South Atlantic, which experiences higher SST and surface air temperature. The suppression of the NADW also drastically change the atmospheric circulation. At 800 hPa strong high pressure anomaly is predicted over the North Atlantic/Europe whereas low pressure anomalies act over North America and the North Pacific. The high pressure anomaly is a consequence of the North Atlantic cooling that stabilizes the atmosphere. This is apparently caused by weaker cold-ocean fluxes of sensible and latent heat to the atmosphere (Rind (1987)). The associated northward wind anomalies over the North Atlantic increase the warm air advection from the tropics and

induce the transport of tropical saltier water to mid-latitudes. Furthermore, calculation of high pass transient eddy activity demonstrated increased (decreased) low level poleward temperature flux in agreement with higher (lower) baroclinic activity in the NH (SH) (Fig. 11). This negative atmospheric-oceanic feedback should play an important role to resume the NADW after the freshwater forcing ends up. Furthermore, the analyses here showed that wind anomalies act as a negative feedback to the initial freshwater forcing.

Comparing the FI experiments with proxy data reveals a general agreement. For instance, Grootes and Stuiver (1997) inferred surface temperature in Greenland lower than 20°C compared to today or 3-6°C compared to the LGM. Schäfer et al. (2001)) argued that the meltwater released during the major iceberg armada led to an entire stop in NADW and intermediate-water production as well as a reverse pattern of THC, which in turn, reduces the heat transported northward. Therefore, the inferred climate changes from paleo proxy data have been satisfactorily reproduced in the FI experiments discussed here. The comparison with other modeling results, however, is more complicated since the most part of experiments have been set up with present day boundary conditions (Rind et al. (2001a), Rind et al. (2001b), Manabe and Stouffer (2000),Schiller et al. (1997)).

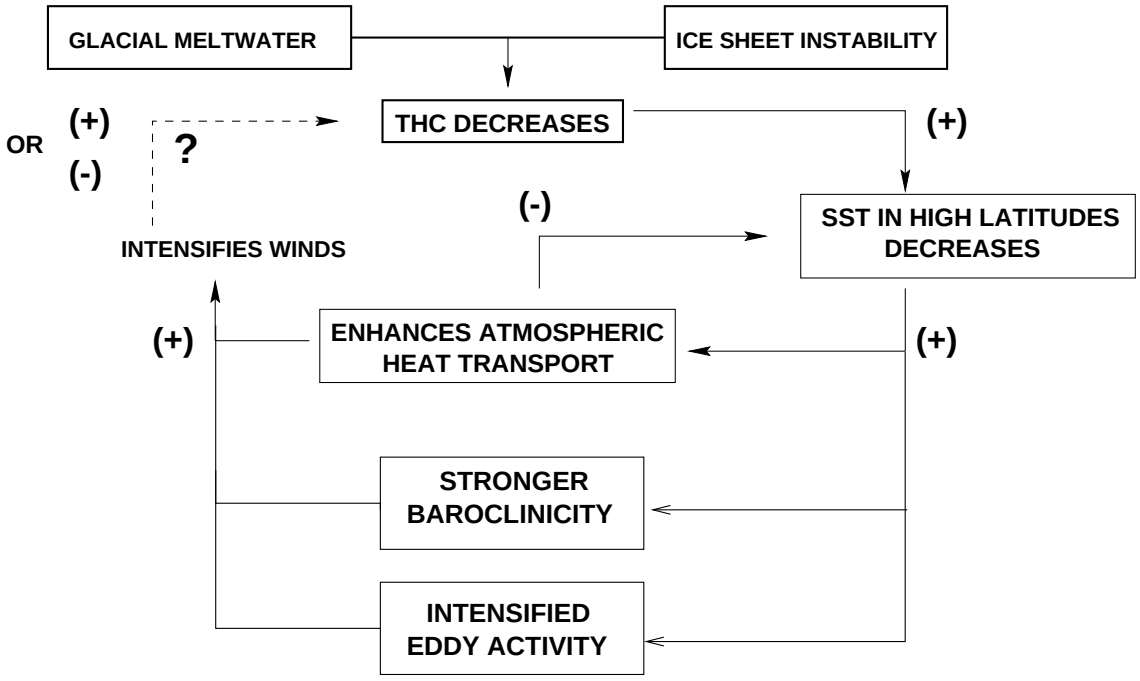

Figure 1: Air-sea mechanism explored in this paper. $(+)$ and $(-)$ indicate positive and negative feedbacks

Experiments	Total Heat	Global Ocean	Atl.	Indi./Pac.	Atmosphere
LGM	5.17	1.25	1.01	0.24	3.92
$0.19FI$	5.01	1.13	0.87	0.26	3.88
$0.38FI$	4.84	1.00	0.72	0.28	3.84
$0.47FI$	4.56	0.62	0.06	0.56	3.94

Table 1: Time averaged heat transport at 30°N for the FI experiments and the LGM run [PW]. The atmosphere heat transport is calculated as the difference between the total heat transport and the oceanic contribution.

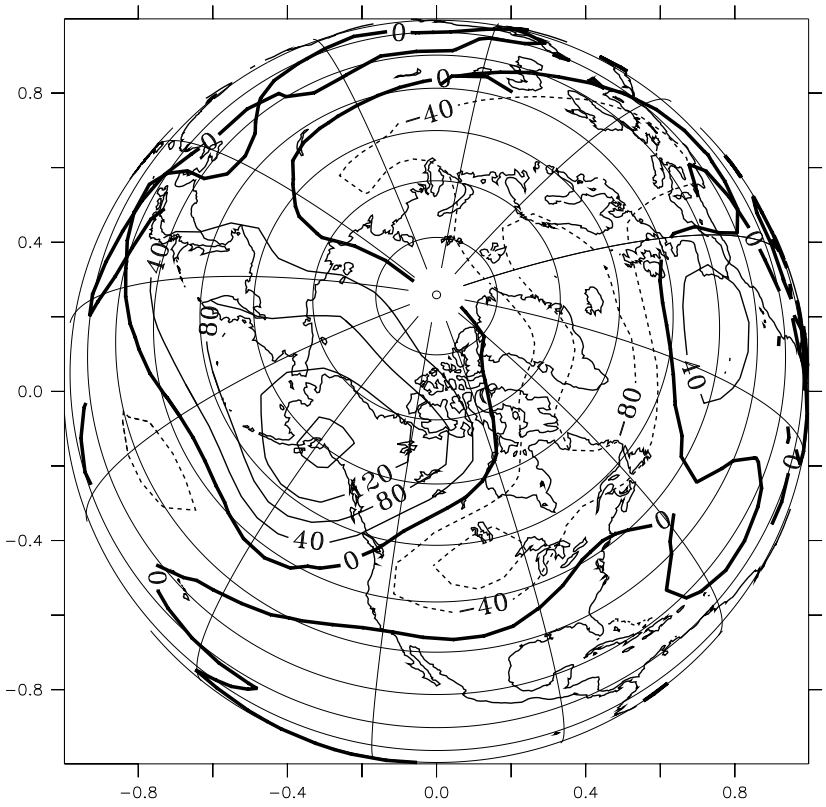

Figure 2: DJF eddy geopotential height anomalies at 500 hPa between the LGM and the present day run [$m^2 s^{-2}$].

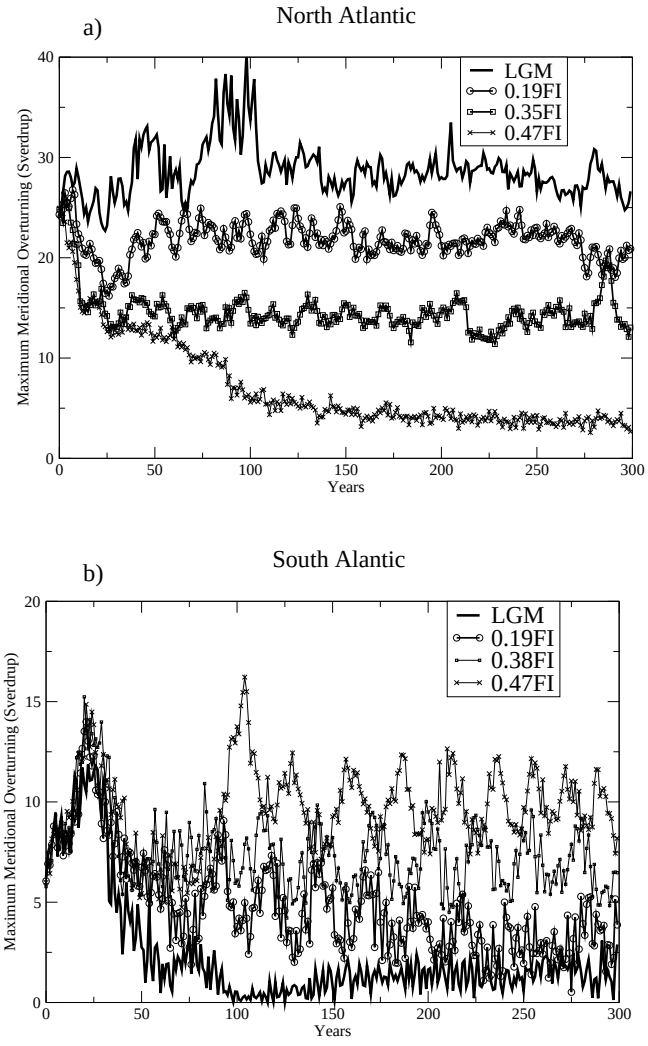

Figure 3: Time averaged maximum meridional overturning in the North Atlantic for freshwater experiments and LGM run [Sv] (a). And (b) is AABW exported northward at 20°S in the South Atlantic for the FI and LGM experiments.

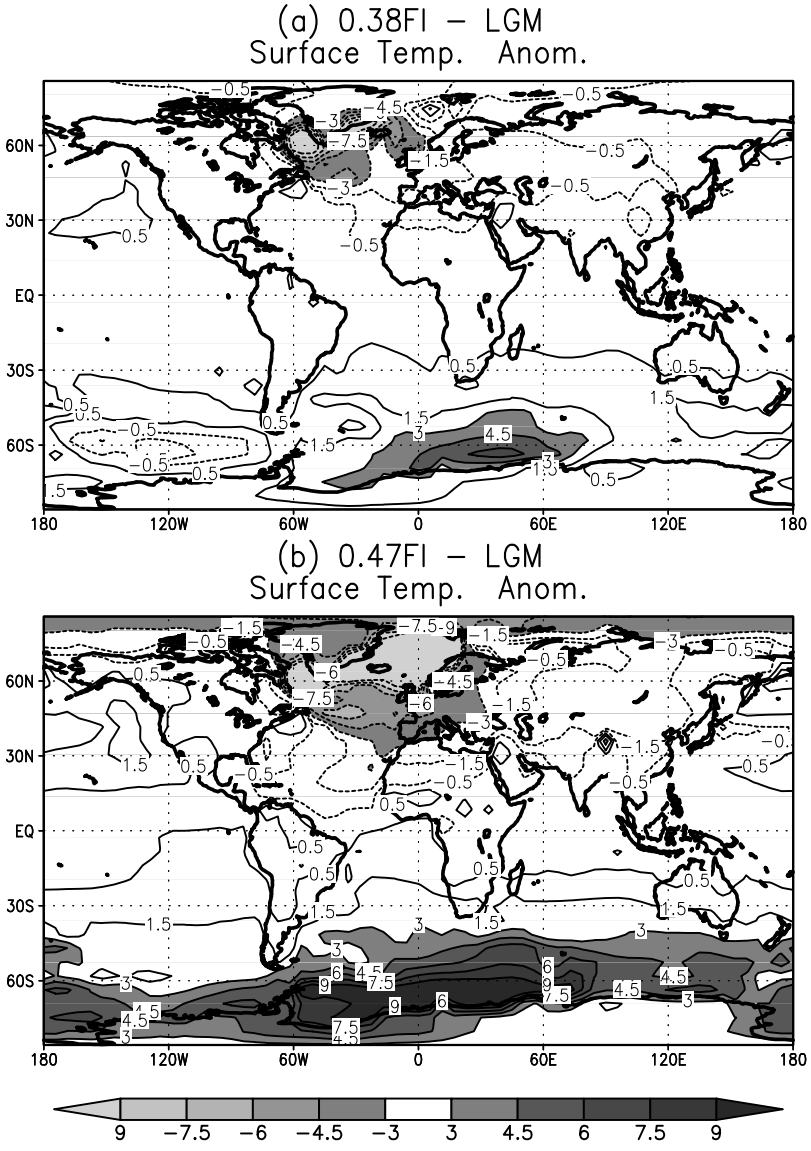

Figure 4: Time averaged surface temperature anomalies between the FI experiments and LGM run. (a) 0.38FI (b) 0.47FI. [°C].

(a) 0.38FI − LGM
Geopg. Height Anom. at 800hPa [m]

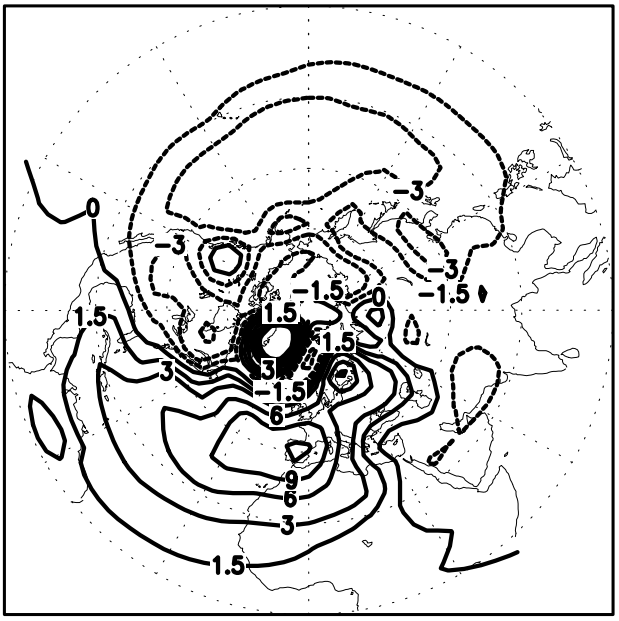

(b) 0.47FI − LGM
Geopg. Height Anom. at 800hPa [m]

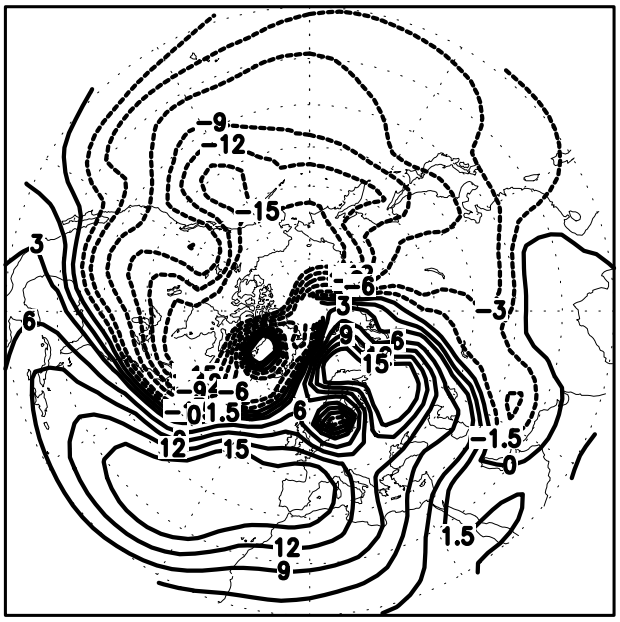

Figure 5: Similar Fig. 4 but for geopotential height [m].

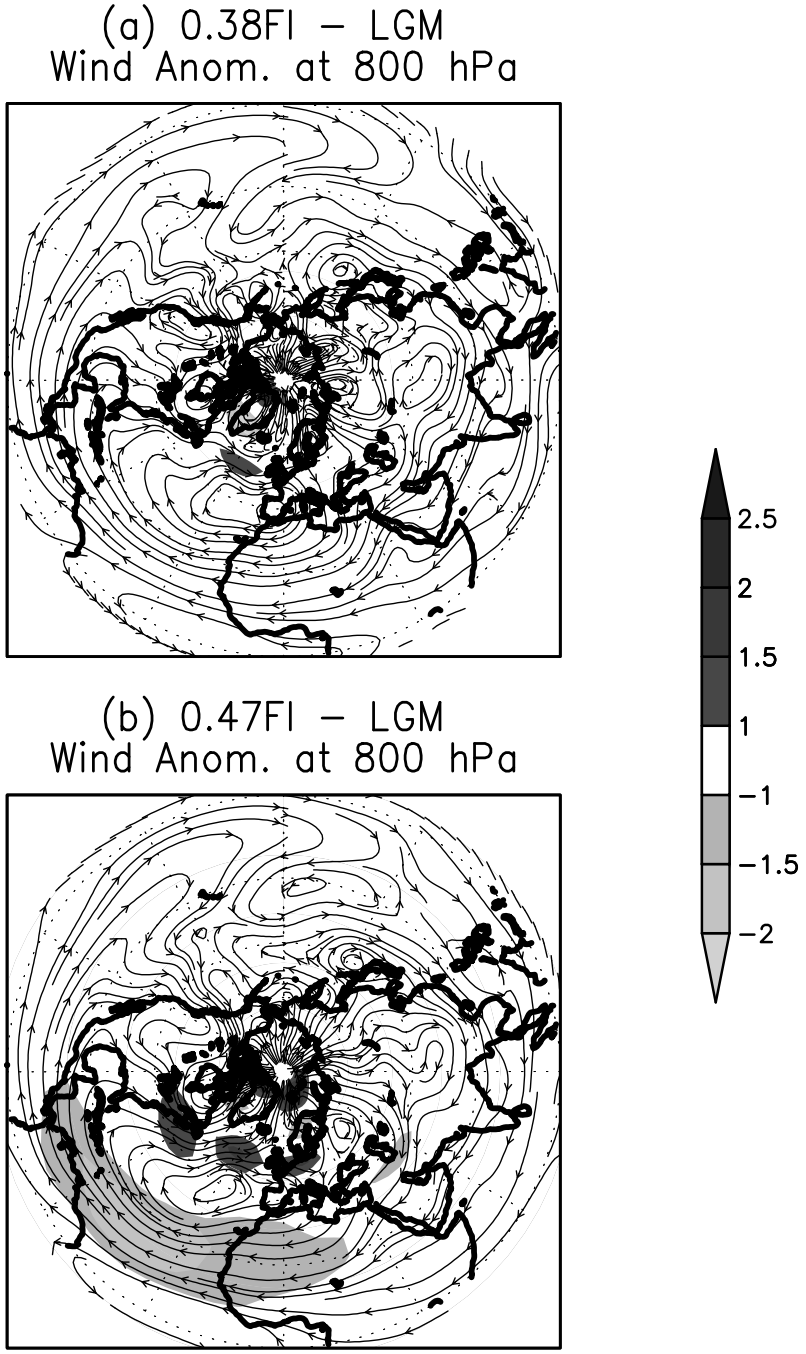

Figure 6: Similar Fig. 4 but for winds at 800 hPa [m/s]. Values larger (smaller) than 1m/s (-1m/s) are shaded.

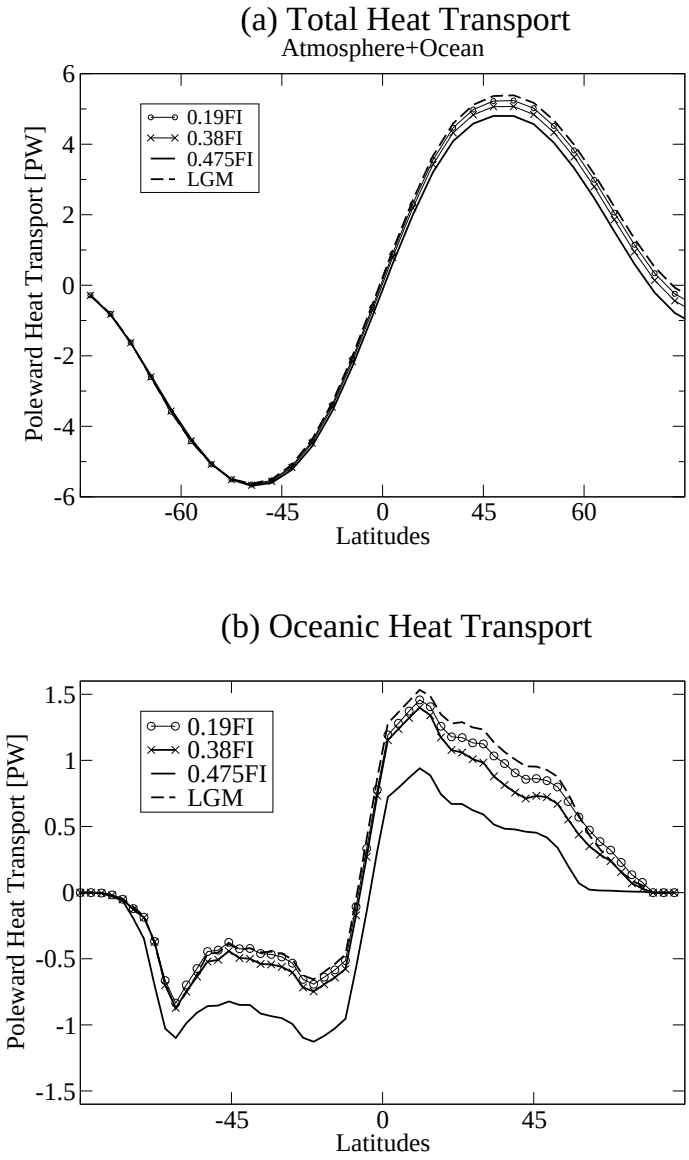

Figure 7: Time averaged total heat transport (atmosphere+ocean) for the LGM and FI experiments (a). And (b) the oceanic heat transport [PW].

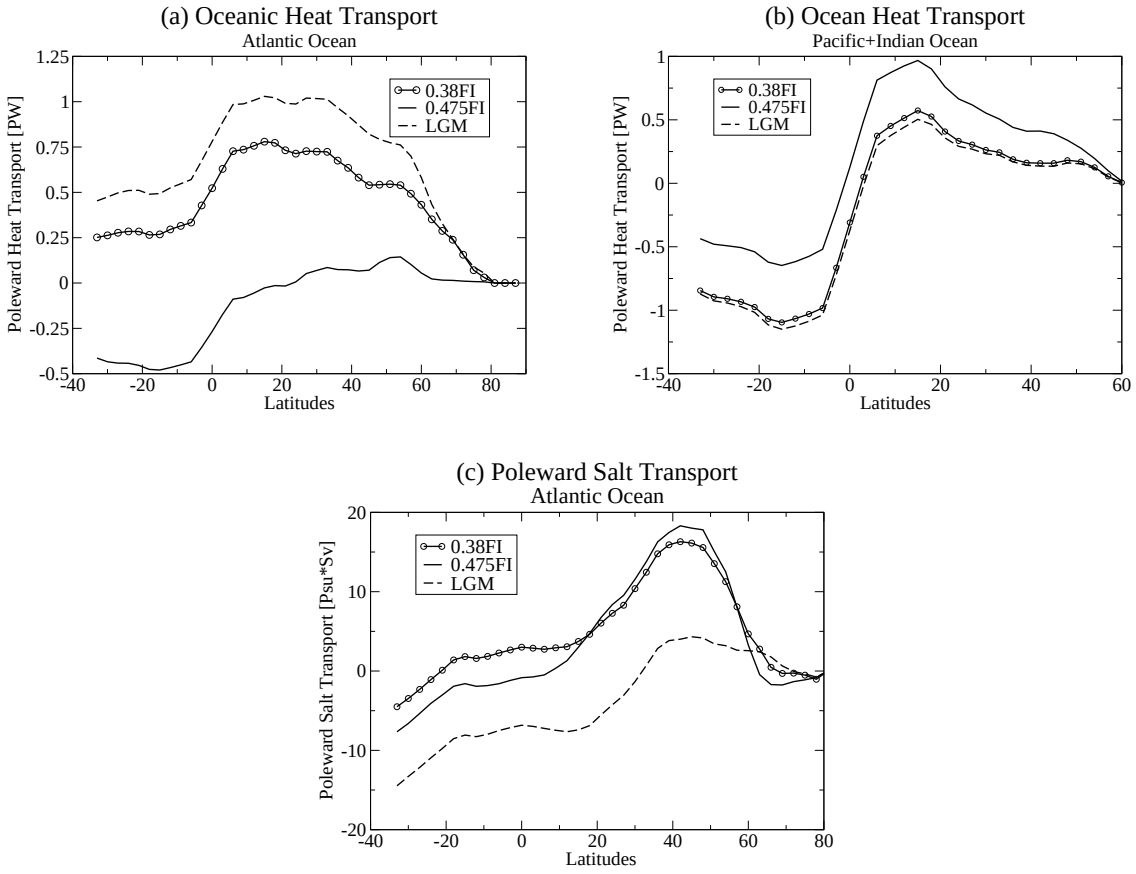

Figure 8: Time averaged oceanic heat transport [PW] for the LGM and FI experiments in Atlantic (a), Indian/Pacific sector (b). (c) is the poleward salt transport in Atlantic [psuSv].

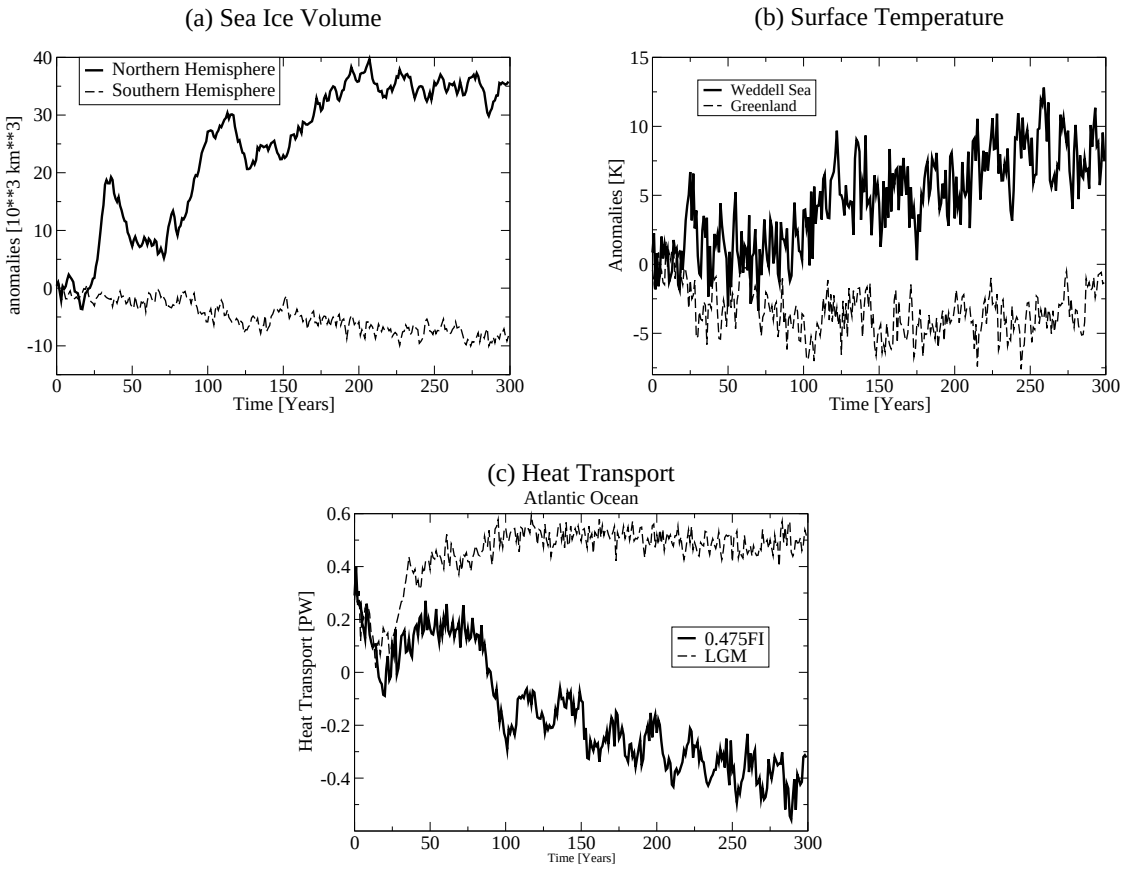

Figure 9: Time evolution of sea-ice volume anomalies between 0.47FI experiment and LGM run [$10^3 \times km^3$] (a), and Surface temperature [°C] in Greenland and Weddell Sea (b). (c) is the time evolution of the northward heat transport in Atlantic at 30°S [PW].

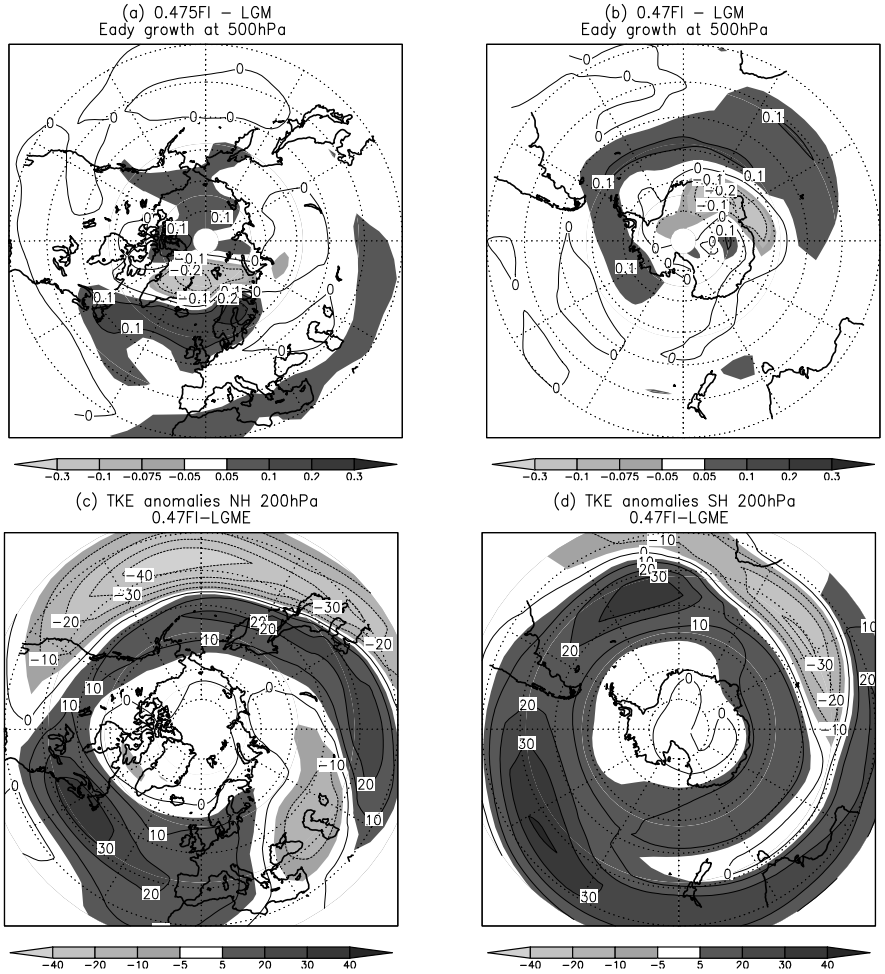

Figure 10: Time averaged Eady growth rate anomalies between 0.47FI and LGM (a) NH, and (b) SH [day^{-1}]. (c) and (d) is the same as (a) and (b) but for the total kinetic energy anomalies at 200 hPa [$m^2 s^{-2}$].

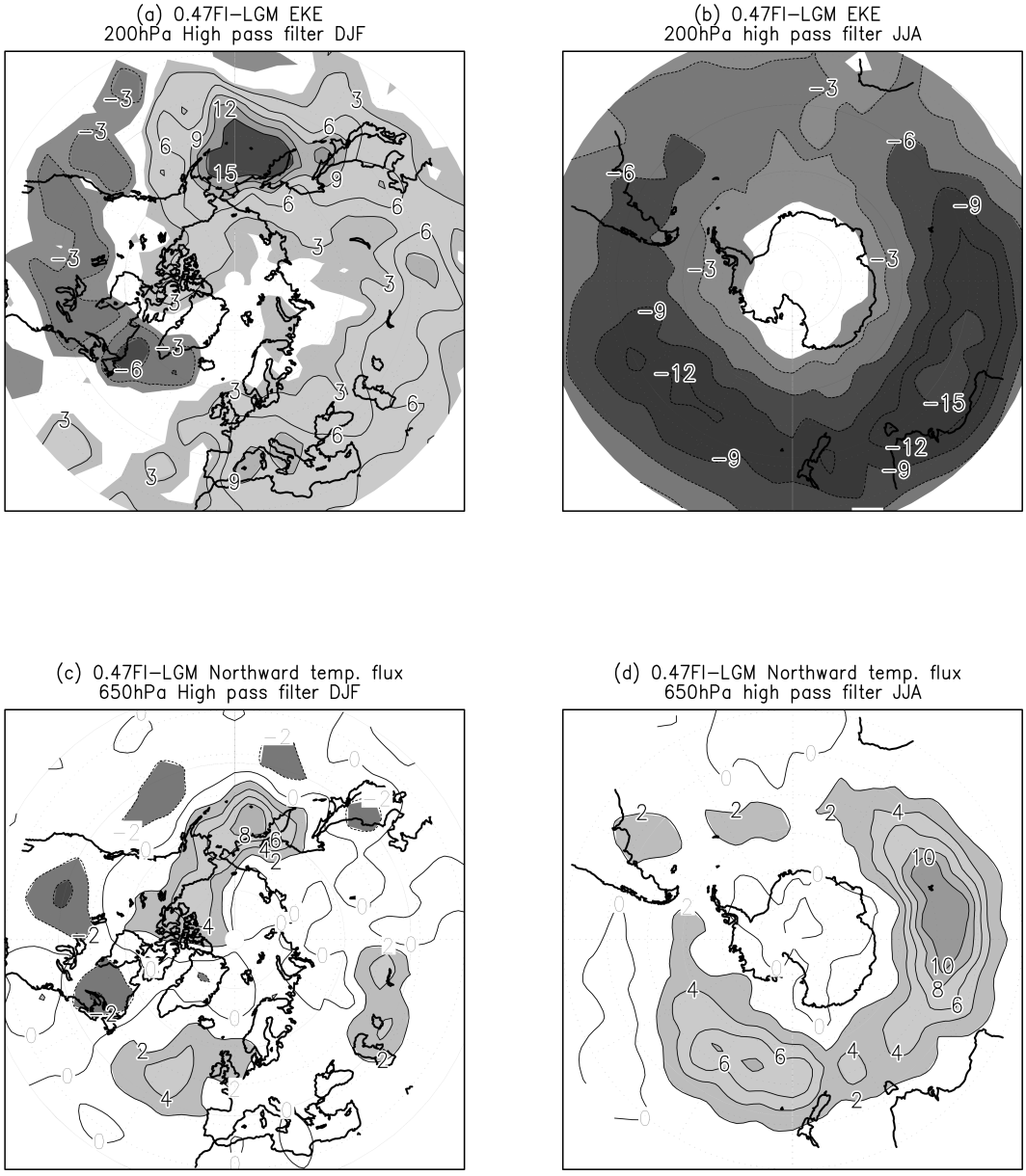

Figure 11: DJF high pass transient kinetic energy anomalies between 0.47FI and LGM at 200 hPa in the NH (a) and in the SH (b). (c) and (d) the same as (a) and (b) but for high pass transient temperature flux at 650 hPa [$K \times ms^{-1}$].

5. acknowledgments

I am grateful to Prof. A. Timmermann and Prof. W.R. Peltier for their fruitful comments, suggestions and overall support.

References

Alley, R., 2000: Ice-core evidence of abrupt climate changes. *Proceedings of the National Academy of Sciences*, National Academy of Sciences, volume 97, 1331–1334.

Berger, A., 1978: A simple algorithm to compute long-term variations of daily and monthly insolation. Technical Report 18, Institut d'astronomique et de géophysique, Université de Lauvain.

Bjerknes, J., 1964: Atlantic air-sea interaction. *Advances in Geophysics*, **10**, 1–82.

Blunier, T. and E. Brook, 2001: Timing of millenial-scale climate change in Antarctica and Greenland during the last glacial period. *Science*, **291**, 109–112.

Blunier, T., J. Chappellaz, J. Schwander, A. Dällenbach, B. Stauffer, T. Stocker, D. Raynaud, J. Jouzel, H. Clausen, C. Hammer, and S. Johnsen, 1998: Asynchrony of Antarctic and Greenland climate change during the last glacial period. *Nature*, **394**, 739–74.

Bond, G., W. Showers, M. Chesebiet, M. Lotti, R. Almasi, P. deMenocal, P. Priore, P. Cullen, H. Hajdas, and G. Bonani, 1997: A pervasive Millennial-scale cycle in North Atlantic Holocene and glacial climates. *Science*, **278**, 1257–1266.

Böning, C., F. Bryan, W. Holland, and R. Döscher, 1996: Deep-water formation and meridional overturning in a high-resolution model of the North Atlantic. *J. Phys. Oceanogr.*, **26**, 1142–1164.

Broecker, S., 1994: Massive iceberg discharges as triggers for global climate change. *Nature*, **372**, 421.

Broecker, W., 1995: *The glacial world according to Wally*. Eldigio Press, New York, USA.

— 1998: Paleocean circulation during the last deglaciation. A bipolar seesaw? *Paleoceanography*, **13**, 119–121.

Campin, J. and H. Goosse, 1999: A parameterization of dense overflow in large-scale ocean models in z coordinate. *Tellus*, **51A**, 412–430.

CLIMAP, 1981: Seasonal reconstruction of the Earth's surface of the last glacial maximum. . *Geol. Soc. Am. Map. Chart Ser.*, **MC-36**, 1–18.

Cook, K. and I. Held, 1988: Stationary waves of the ice age climate. *J. Climate*, **1**, 807–819.

Crowley, T., 1995: Ice age terrestrial carbon changes revisited. *Global Biogeochemical Cycles*, **9**, 377–389.

Crucifix, M., M. Loutre, and P. Tulkens, 2002: Climate evolution during the Holocene: a study with an Earth system model of intermediate complexity. *Clim. Dyn.*, **19**, 43–60.

Gent, P. and J. McWilliams, 1990: Isopycnal mixing in ocean general circulation models. *J. Phys. Oceanogr.*, **20**, 150–155.

Goosse, H., E. Deleersnijder, T. Fichefet, and M. England, 1999: Sensitivity of a global coupled ocean-sea ice model to the parameterization of vertical mixing. *J. Geophys. Res.*, **104(C6)**, 13681–13695.

Goosse, H. and T. Fichefet, 1999: Importance of ice-ocean interactions for the global ocean circulation: a model study. *J. Geophys. Res.*, **104(C10)**, 23337–23355.

Goosse, H., F. Selten, R. Haarsma, and J. Opsteegh, 2002: Large sea-ice volume anomalies simulated in a coupled climate model. *Clim. Dyn.*, **10**, DOI: 10.1007/s00382–002–0290–4.

Grootes, P. and M. Stuiver, 1997: Oxygen 18/16 variability in greenland snow and ice with $10-3$ and $10-5$ year time resolution. *J. Geophys. Res.*, **C102**, 26455–26470.

Hall, M. and H. Bryden, 1982: Direct estimates of ocean heat transport. *Deep Sea Res.*, **29**, 339–359.

Held, I. and M. Suarez, 1978: A two-level primitive equation atmosphere model designed for climate sensitivity experiments. *J. Atmos. Sci.*, **35**, 206–229.

Hewitt, C. D., A. Broccoli, J. Mitchell, and R. J. Stouffer, 2001: A coupled model of the last glacial maximum: was part of the North Atlantic relatively warm? *Geophys. Res. Lett.*, **28**, 1571–1574.

Houghton, E. J. T., Y. Ding, D. Griggs, M. Noguer, P. V. Linden, X. Dai, K. Maskell, and C. A. Johnson., eds., 2001: *Climate Change 2001. The scientific basis*. Cambridge Univ. Press., Cambridge, U.K., pps. 881 pp.

Justino, F., 2004: *The influence of glacial boundary conditions on the climate system during the Last Glacial Maximum*. Ph.D. thesis, Leibniz Institute of Marine Research, Kiel, Germany.

Justino, F., A. Timmermann, U. Krebs, and E. Souza, 2005: Synoptic reorganisation of atmospheric flow during the last glacial maximum. *J. Climate.*, in press.

Kitoh, A., S. Muakami, and H. Koide, 2001: A simulation of the Last Glacial Maximum with a coupled atmosphere-ocean GCM. *Geophys. Res. Lett.*, **28**, 2221–2224.

Knutti, R., J. Flueckiger, T. Stocker, and A. Timmermann, 2004: Strong hemispheric coupling of glacial climate through continental freshwater discharge and ocean circulation. *Nature*, **430**, 851–856.

Kohlfeld, K. and S. Harrison, 2000: How well can we simulate past climates? Evaluating the models using palaeoenvironmental datasets. *Quat. Sci. Rev.*, **19**.

Liccard, J., J. Teller, and P. Clark, 1999: Freshwater routing by the Laurentide ice sheet during the last deglaciation. *Mechanisms of Millenial-scale Global Climate Change*, in AGU Monograph.

Lindzen, R. and B. Farrell, 1980: A simple approximate result for maximum growth rate of baroclinic instabilities. *J. Atmos. Sci.*, **37**, 1648–1654.

MacAyeal, D., 1993: Binge/purge oscillations of the Laurentide ice sheet as a cause of the North Atlantic's Heinrich events. *Paleoceanography*, **8**, 775–784.

Manabe, S. and R. Stouffer, 1997: Coupled ocean-atmosphere model response to freshwater input: comparison to younger dryas event. *Nature*, **12**, 321–336.

Manabe, S. and R. J. Stouffer, 1995: Simulation of abrupt climate change induced by freshwater input to the North Atlantic Ocean. *Nature*, **378**, 165–167.

— 2000: Study of abrupt climate change by a coupled ocean-atmosphere model. *Quaternary Science Reviews*, **19**, 285–299.

Marotzke, J. and P. H. Stone, 1995: Atmospheric Transport, The Thermohaline Circulation, and Flux Adjustments in Simple Coupled Model. *J. Phys. Oceanogr.*, **25**, 1350–136.

Marshall, J. and F. Molteni, 1993: Toward a dynamic understanding of planetary-scale flow regimes. *J. Atmos. Sci.*, **50**, 1792–1818.

Marshall, S. and G. Clarke, 1999: Modeling North American Freshwater Runoff through the Last Glacial Cycle. *Quat. Res.*, **52**, 300–315.

McCave, I., B. Manighetti, and N. Beveridge, 1995: Changes in circulation of the North Atlantic during the last 25,000 years inferred from grain-size measurements. *Nature*, **374**, 149–152.

Mellor, G. and T. Yamada, 1982: Development of a turbulence closure model for geophysical fluid problems. *Rev. Geophys. Space Phys.*, **20**, 851–875.

Mikolajewicz, U., T. Crowley, A. Schiller, and R. Voss, 1997: Modelling teleconnection between the North Atlantic and North Pacific during the Dryas event. *Nature*, **387**, 384–387.

Oka, A., H. Hasumi, and N. Suginohara, 2001: Stabilization of thermohaline circulation by wind-driven and vertical diffusive salt transport. *Clim. Dyn.*, **18**, 71–83.

Opsteegh, J., R. Haarsma, F. Selten, and A. Kattenberg, 1998: ECBILT: A dynamic alternative to mixed boundary conditions in ocean models. *Tellus*, **50A**, 348–367.

Peixoto, J. and A. Oort, 1992: *Physics of Climate*. Spring-Verlag, 520 pp.

Peltier, W., 1994: Ice age paleotopography. *Science*, **265**, 195–201.

Rind, D., 1987: Components of the ice age circulation. *J. Geophys. Res*, **92**, 4241–4281.

Rind, D., P. Demenocal, G. Russell, S. Sheth, D. Collins, G. Schmidt, and J. Teller, 2001a: Effects of glacial meltwater in the GISS Coupled Atmosphere-Ocean Model: Part I: North Atlantic Deep Water Response. *J. Geophys. Res.*, **106**, 27335–27354.

Rind, D., G. Russell, G. Schmidt, S. Sheth, D. Collins, P. Demenocal, and J. Teller, 2001b: Effects of glacial meltwater in the GISS Coupled Atmosphere-Ocean Model: Part II: A bi-polar seesaw in Atlantic Deep Water production. *J. Geophys. Res.*, **106**, 27355–27366.

Schäfer, P., W. Ritzrau, M. Schlüter, and J. Thiede, eds., 2001: *Fundamental modes and abrupt changes in North Atlantic circulation and climate over the last 60 ky - Concepts, reconstructions and numerical modeling*, Springer Verlag, Berlin. 365–410.

Schäfer-Neth, C. and A. Paul, 2003: Gridded global lgm sst and salinity reconstruction. *IGPB Pages/World Data Center for Paleoclimatology*, data Contribution Series 2003-046.

Schiller, A., U. Mikolajewicz, and R. Voss, 1997: The stability of the North Atlantic thermohaline circulation in a coupled ocean-atmosphere general circulation model. *Clim. Dyn.*, **13**, 325–347.

Schmitt, R., P. Bogden, and C. Dorman, 1989: Evaporation minus precipitation and density flux for the North Atlantic. *J. Phys. Oceanogr.*, 1208–1221.

Schneider, S. H., ed., 1996: *Encyclopedia of Climate and Weather*. Oxford University Press, 278-283 pp.

Seidov, D., E. Barron, and B. Haupt, 2001: Meltwater and the global conveyor: northern versus southern connections. *Global Planetary Change*, **30**, 257–270.

Speer, K. and E. Tziperman, 1992: Rates of water mass formation in the North Atlantic Ocean. *J. Phys. Oceanogr.*, **22**, 94–104.

Stocker, T. and S. Johnsen, 2003: A minimum thermodynamic model for a bipolar seesaw. *Paleoceanography*, **18**, doi:10.1029/2003PA000920.

Stocker, T. F., 1998: The seesaw effect. *Science*, **286**, 61–62.

Talley, D., 2003: Shallow, intermediate, and deep overturning components of the global heat budget. *J. Phys. Oceanogr.*, **35**, 530–560.

Talley, D., L. Reid, and E. Robbins, 2003: Data-based meridional overturning streamfunctions for the global ocean. *J. Climate*, **16**, 3213–3226.

Timmermann, A. and H. Goosse, 2004: Is the wind stress forcing essential for the meridional overturning circulation. *Geophys. Res. Lett.*, **31**.

Timmermann, A., F. Justino, F.-F. Jin, U. Krebs, and H. Goosse, 2004: Surface temperature control in the North and tropical Pacific during the last glacial maximum. *Clim. Dyn.*, **23**, 353–370.

Trenberth, K., 1991: Storm tracks in the southern hemisphere. *J. Atmos. Sci.*, **48**, 2151–2178.

Trenberth, K. and J. Caron, 2001: Estimates of meridional atmosphere and ocean heat transports. *J. Climate*, **14**, 3433–3443.

Veum, T., E. Jansen, M. Arnold, I. Beyer, and J. Duplessy, 1992: Water mass exchange between the North Atlantic and the Norwegian Sea during the past 28,000 years. *Nature*, **356**, 783–785.

von Grafenstein, U., H. Erlenkeuser, J. Muller, J. Jouzel, and S. Johnson, 1998: The cold event 8,200 years ago documented in oxygen isotope records of precipitation in Europe and Greenland. *Clim. Dyn*, **14**, 73–81.